Cluster Synchronization in Multilayer Networks: A Fully Analog Experiment with *LC* Oscillators with Physically Dissimilar Coupling

Karen A. Blaha,[1,*] Ke Huang,[2] Fabio Della Rossa,[1,3] Louis Pecora,[4] Mani Hossein-Zadeh,[2] and Francesco Sorrentino[1,2]
[1]*Department of Mechanical Engineering, University of New Mexico, Albuquerque, New Mexico 87131, USA*
[2]*Department of Electrical and Computer Engineering, University of New Mexico, Albuquerque, New Mexico 87131, USA*
[3]*Politecnico di Milano, Piazza Leonardo da Vinci 32, 20133 Milano, Italy*
[4]*U.S. Naval Research Laboratory, Washington, DC 20375, USA*

(Received 14 July 2018; published 4 January 2019)

We investigate cluster synchronization in experiments with a multilayer network of electronic Colpitts oscillators, specifically a network with two interaction layers. We observe and analytically characterize the appearance of several cluster states as we change coupling in the layers. In this study, we innovatively combine bifurcation analysis and the computation of transverse Lyapunov exponents. We observe four kinds of synchronized states, from fully synchronous to a clustered quasiperiodic state—the first experimental observation of the latter state. Our work is the first to study fundamentally dissimilar kinds of coupling within an experimental multilayer network.

DOI: 10.1103/PhysRevLett.122.014101

Networks with multiple layers of interactions arise in models for epidemic propagation [1,2], the social world of the Medicis [3], and the failure of interdependent networks such as the power grid [4,5], among others. These layers of interactions can operate in fundamentally different ways. Neurons communicate by both chemical and electrical coupling; chemical synapses are probabilistic, delayed, and unidirectional while electrical synapses are deterministic and bidirectional [6]. The interplay between both kinds of synapses is thought to be essential to normal functioning of the brain [6–8].

Networks with a high number of symmetries arise in many systems [9]: in biology, the *C. elegans* metabolic network; in infrastructure, the U.S. power grid and airport network; in social networks, the Ph.D. network [10]. Symmetric multilayer networks have been investigated using quotient networks for dimensionality reduction [11,12] and using eigenspectral analysis [11]. Study of synchronization in multilayer networks was originally presented in Refs. [13,14] and more recently in Ref. [15]. Recent experiments explored synchronization between identical [16] and nonidentical [17] layers of a multilayer network. These papers studied complete synchronization (all systems synchronizing on the same time evolution) with only diffusive coupling.

Clustered patterns arise from network symmetries [18,19], but few experiments study this causality; most experimental studies focus solely on the appearance of interesting clusters and not on the role the network symmetries play in their presence [20–22]. The studies that do directly connect network symmetry and clustering are digitally implemented [18,23,24]; they exclude some aspects that arise in real systems. No experimental study of clustering in multilayer networks exists.

In this Letter, we are the first to study cluster synchronization in a fully analog symmetrical multilayer network with both diffusive and nondiffusive coupling. Despite its simplicity, this analog electronic system not only represents the smallest multilayer network with multiple symmetries but also captures the uncertainties and fluctuations present in real and more complex physical systems. We describe the possible cluster synchronizations of the system as we vary coupling parameters. We experimentally observe and theoretically characterize clusters of nodes that synchronize on different time evolutions. The system is fully analog, where other studies have used a computer interface to implement coupling [16,17,25].

Electronic circuits are ideal test beds for the study of nonlinear behavior in networks [26]; we choose to use the Colpitts oscillator. As shown in the left-hand panel of Fig. 1,

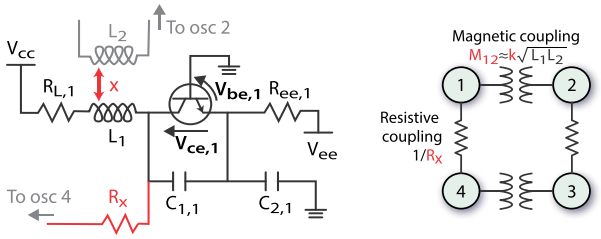

FIG. 1. Left: Colpitts oscillator. The oscillator is coupled to its two neighbors via resistor R_x and mutual magnetic coupling between the tank inductors, controlled by the inductor separation x. Tunable parameters are in red, fixed components of other oscillators are in gray. Right: Topology of the coupled oscillator network. $M_{ij} = k\sqrt{L_iL_j}$, where k is roughly proportional to $1/x^2$.

the Colpitts oscillator is a simple electronic oscillator based on a bipolar junction transistor (BJT) that uses two center-tapped capacitors in series with a parallel inductor as its resonance tank circuit. Several studies have explored the periodic, quasiperiodic, and chaotic behavior of individual Colpitts oscillators [27–30]. Others have discussed either magnetically coupled [31] or resistively coupled [30] Colpitts oscillators. Simplicity, low cost, ease of fabrication, ability to work in different regimes, availability of a large volume of previous studies, and the ability to introduce different kinds of connections make the Colpitts oscillator particularly suitable for multilayer network studies. We create the first fully analog multilayer network with four periodic Colpitts oscillators coupled through two different kinds of coupling mechanisms, resistive and magnetic.

The right-hand panel of Fig. 1 shows the topology of the corresponding network; this is the simplest multilayer network that has multiple symmetries [for an easier network with only one symmetry, see Supplemental Material (SM), Sec. II [32]]. The four nodes, each a Colpitts oscillator, form a ring with coupling alternating between resistive and magnetic. We achieve resistive coupling by connecting the collectors of transistors in pairs of oscillators through a resistor R_x; we tune the coupling by connecting resistors of the desired value. To achieve magnetic coupling, we bring the inductors of two nodes sufficiently near, such that the mutual inductance M_{ij} becomes large enough; we tune the coupling by changing the inductor separation distance x.

The dynamics of the network shown in Fig. 1 is

$$\begin{aligned}
C_{1,i}\dot{V}_{ce,i} &= I_{L,i} - I_c(V_{be,i}) \\
&\quad + \frac{1}{R_x}\sum_{j=1}^{N}\mathbb{R}_{ij}[(V_{ce,j}-V_{ce,i})-(V_{be,j}-V_{be,i})], \\
C_{2,i}\dot{V}_{be,i} &= -(V_{ee}+V_{be,i})/R_{ee,i} - I_b(V_{be,i}) - I_{L,i} \\
&\quad - \frac{1}{R_x}\sum_{j=1}^{N}\mathbb{R}_{ij}[(V_{ce,j}-V_{ce,i})-(V_{be,j}-V_{be,i})], \\
L_i\dot{I}_{L,i} &= V_{cc} - V_{ce,i} + V_{be,i} - I_{L,i}R_{L,i} - \sum_{j=1}^{N} M_{ij}\mathbb{M}_{ij}\dot{I}_{L,j},
\end{aligned} \tag{1}$$

where $i = 1, \ldots, 4$ is the index of the oscillator, L_i is the inductance, $C_{1,i}$, $C_{2,i}$ are the capacitances of the circuit components (see Fig. 1), $V_{ce,i}$ is the voltage drop between the collector and the emitter of the transistor, and $V_{be,i}$ is the voltage drop between the base and the emitter. V_{cc} and V_{ee} are applied voltages, I_b and I_c are the current of the base and the collector, respectively. These two currents are the nonlinear terms in the system; they are zero below a threshold voltage and increase linearly above this cutoff. In a BJT these currents are related through $\beta = \Delta I_c/\Delta I_b \approx I_c/I_b$, where β is the BJT amplification factor, see SM, Sec. I for more details about the experimental arrangement [32].

The magnitudes of the resistive and magnetic coupling coefficients are $1/R_x$ and $M_{ij} = k\sqrt{L_i L_j}$, respectively. k characterizes the mutual inductance and is roughly proportional to $1/x^2$ (see SM for a specific relationship [32]); k is positive if the currents induced by mutual and self-inductance are in phase and negative if they are antiphase. Note that the resistive and magnetic couplings are different in nature and therefore enter the dynamic equations in different forms [as evident in Eq. (1)]. Resistive coupling is diffusive and affects the current. Magnetic coupling is nondiffusive, differential [39], and affects the voltage. The adjacency matrices $\mathbb{R}$ and $\mathbb{M}$ describe how the oscillators are connected to one another by resistive and magnetic coupling, respectively. In our four-member ring network, $\mathbb{R}$ and $\mathbb{M}$ are

$$\mathbb{R} = \begin{bmatrix} 0 & 0 & 0 & 1 \\ 0 & 0 & 1 & 0 \\ 0 & 1 & 0 & 0 \\ 1 & 0 & 0 & 0 \end{bmatrix}, \qquad \mathbb{M} = \begin{bmatrix} 0 & 1 & 0 & 0 \\ 1 & 0 & 0 & 0 \\ 0 & 0 & 0 & 1 \\ 0 & 0 & 1 & 0 \end{bmatrix}. \tag{2}$$

By inspection of the four-node system (right-hand panel of Fig. 1), we observe three symmetries present in the multilayer network, i.e., three permutations of the nodes which leave the network unchanged: (1) vertical symmetry, permuting 1 with 4 and 2 with 3, (2) 180° rotation, permuting 1 with 3 and 2 with 4, and (3) horizontal symmetry, permuting 1 with 2 and 3 with 4. These permutations, along with the identical permutation (that maps each node to itself), form a mathematical group $\mathcal{G}$ that we call *the symmetry group of the multilayer network*. Subgroups of $\mathcal{G}$ define possible cluster patterns [25].

By assuming the Colpitts oscillators have identical components ($C_{1,i}=C_{2,i}=C$, $L_i=L$, $M_{ij}=M_{ji}=M=kL$), we can rewrite Eq. (1) as a generic multidimensional network with $N = 4$ oscillators coupled through $\Lambda = 2$ layers [13–15,40,41] (see SM for derivation [32]):

$$\dot{\boldsymbol{x}}_i = F(\boldsymbol{x}_i) + \sum_{\lambda=1}^{\Lambda}\sigma^{(\lambda)}\sum_{j=1}^{N} A_{ij}^{(\lambda)} H^{(\lambda)}(\boldsymbol{x}_j), \tag{3}$$

where

$$\boldsymbol{x}_i = \begin{bmatrix} V_{ce,i} \\ V_{be,i} \\ I_{L,i} \end{bmatrix}, \quad F = \begin{bmatrix} \frac{-I_c(V_{be,i})+I_{L,i}}{C} \\ \frac{-(V_{ee}+V_{be,i})/R_{ee}-I_b(V_{be,i})-I_{L,i}}{C} \\ \frac{V_{cc}-V_{ce,i}+V_{be,i}-I_{L,i}R_L}{L(1-k^2)} \end{bmatrix},$$

$$H^{(1)} = \begin{bmatrix} V_{ce}-V_{be} \\ V_{be}-V_{ce} \\ 0 \end{bmatrix}, \quad H^{(2)} = \begin{bmatrix} 0 \\ 0 \\ V_{cc}-V_{ce}+V_{be}-I_L R_L \end{bmatrix},$$

$\sigma^{(1)} = 1/CR_x$, $\sigma^{(2)} = -[k/L(1-k^2)]$, $A^{(1)} = \mathbb{R} - I_4$, and $A^{(2)} = \mathbb{M}$, where I_4 is the four-dimensional identity matrix.

Let the clustered motion have C clusters, $\mathcal{C}_1, \ldots, \mathcal{C}_C$, and let $\boldsymbol{s}(t) = s_1(t), s_2(t), \ldots, s_C(t)$ be a possible clustered solution. We can linearize Eq. (3) around that solution, obtaining

$$\delta\dot{\boldsymbol{x}} = \left\{ \sum_{n=1}^{C} E_n \otimes DF(s_n) + \sum_{\lambda=1}^{\Lambda} \sigma^{(\lambda)} (A^{(\lambda)} \otimes I_3) \sum_{n=1}^{C} [E_n \otimes DH^{(\lambda)}(s_n)] \right\} \delta\boldsymbol{x}, \quad (4)$$

where E_n is a 4×4 matrix which identifies if node i belongs to cluster $\mathcal{C}_n$ [$E_n(i,i) = 1$ if $i \in \mathcal{C}_n$, 0 otherwise]. D represents the Jacobian operator.

Using the coordinate change $\delta\boldsymbol{\eta} = (T \otimes I_3)\delta\boldsymbol{x}$, we convert Eq. (4) from the node coordinate system to the irreducible representation coordinate system. The irreducible representation simultaneously block diagonalizes the permutation matrices in the symmetry group of the multilayer network $\mathcal{G}$; each block is an irreducible representation of the group [42]. Equation (4) becomes

$$\delta\dot{\boldsymbol{\eta}} = \left\{ \sum_{n=1}^{C} J_n \otimes DF(s_n) + \sum_{\lambda=1}^{\Lambda} \sigma^{(\lambda)} (B^{(\lambda)} \otimes I_3) \sum_{n=1}^{C} [J_n \otimes DH^{(\lambda)}(s_n)] \right\} \delta\boldsymbol{\eta}, \quad (5)$$

where $J_n = TE_nT^{-1}$ and $B^{(\lambda)} = TA^{(\lambda)}T^{-1}$. This change of coordinates decouples the dynamics of perturbations along the synchronous manifold from those transverse to it, allowing us to separately analyze each direction [25].

We perform the cluster synchronization analysis in two steps. First, we characterize global behavior along the synchronous manifold by studying the bifurcations of the nonlinear equations for each quotient network [43]. In the quotient network, all the nodes belonging to the same cluster (i.e., synchronized) are represented by one node, since their dynamics and their coupling with other clusters of the network are identical. We compute all the possible solutions by starting simulations from many initial conditions, and we characterize the stability of each solution with a complete bifurcation analysis. We use AUTO07P [44,45] to locate bifurcations and then MATCONT to compute their normal form coefficients [46–48].

Second, we analyze the transverse block of Eq. (5); we compute the Maximum Lyapunov Exponent [49] of the subsystem, evaluating Eq. (5) at each synchronous stable solution $\boldsymbol{s}_n$ for all the possible parameter pairs. We need the global analysis to characterize all the possible solutions along which we compute the variational equation (see SM for a detailed description of the analysis [32]).

Figure 2 shows the four possible cluster patterns. For each pattern, the quotient network dynamics is described by Eq. (3) with a suitable choice of the coupling matrices $A^{(1)}$ and $A^{(2)}$. We also report the matrices T needed for the study of the stability transverse to each synchronous solution. To assess the stability of the clustered solutions, we analyze only the three possible two-cluster quotient networks. The fully synchronized pattern is a special solution of all three two-cluster quotient networks, and we can thus obtain its stability by looking at the stability of each of the other patterns.

In Fig. 3, we show the combined analysis of the three clustered solutions, grouped into in-phase (left) and antiphase (right) solutions (see the SM for a detailed analysis of the three clustered solutions, where we present and explain each bifurcation diagram and transverse stability diagram [32]). We identify nine regions with qualitatively different clustered patterns (reported in the bottom boxes of Fig. 3). We group the cluster patterns to relate them to experimentally observable behavior; this is because some of the cluster states become indistinguishable in the presence of experimental noise and heterogeneity. For example, cluster patterns (a_1) and (a_2) differ by a small phase offset that cannot be measured due to experimental noise. Cluster patterns (a_1) and (a_3) differ mostly in amplitude, but the experimental amplitude is sensitive to many details beyond the scope of the model, such as the resistances of the capacitors, inductors, and component junctions, and nonlinearity of the transistor gain. We thus create four groups

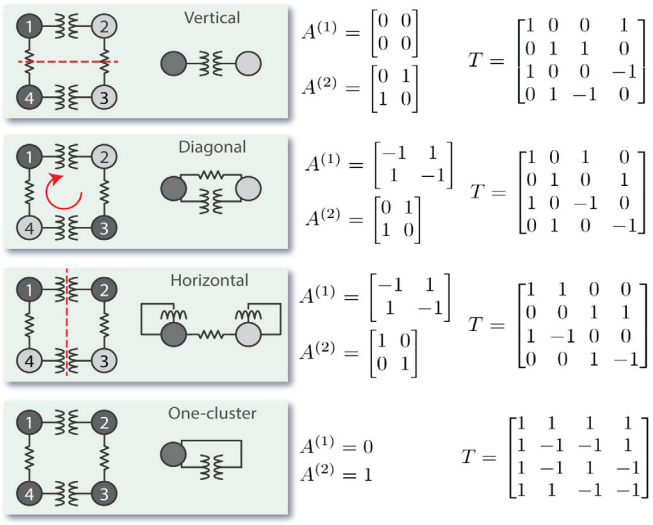

FIG. 2. Possible cluster synchronization patterns. The left-hand schematic represents the full network; nodes belonging to the same cluster synchronization pattern are colored the same. We indicate symmetry with the red dashed line. The one- or two-node labeled schematic represents the quotient network. On the right, we show the $A^{(\lambda)}$ and T for each pattern. $A^{(\lambda)}$ is the adjacency matrix for layer λ, with $\lambda = 1$ representing the resistive layer and $\lambda = 2$ representing the magnetic layer.

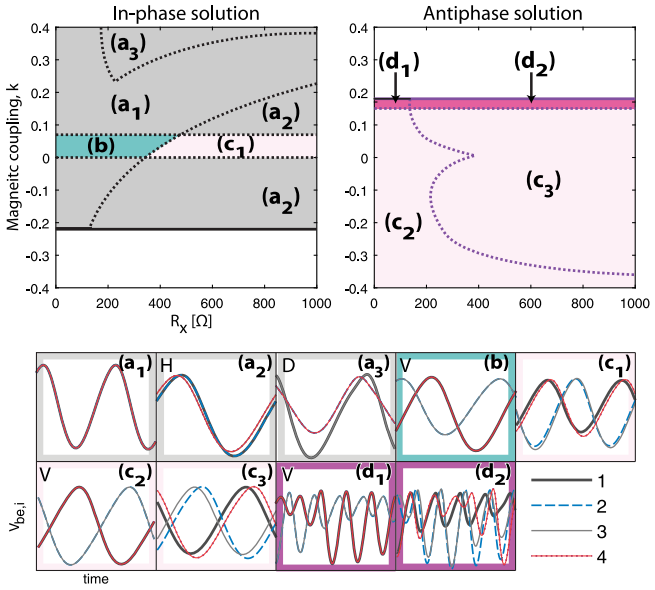

FIG. 3. Possible patterns of Eq. (3). Region coloring indicates experimentally distinguishable patterns: [(a), gray] in-phase, tolerating small mismatches in amplitude and phase; [(b), turquoise] vertical two-cluster with a phase offset up to $\pi/2$ rad; [(c), pink] vertical two-cluster, tolerating small mismatches in amplitude and phase; [(d), magenta] quasiperiodic vertical two-cluster, tolerating small mismatches in amplitude. (Top panels): bifurcation diagram of the (left) in-phase and (right) antiphase solution. (Bottom panels): representative time series of $V_{be}(t)$ from simulations grouped by experimental observability. When clustered solutions are present, we indicate them with V, H, or D in the upper left hand corner for vertically-, horizontally-, and diagonally-synchronized, respectively.

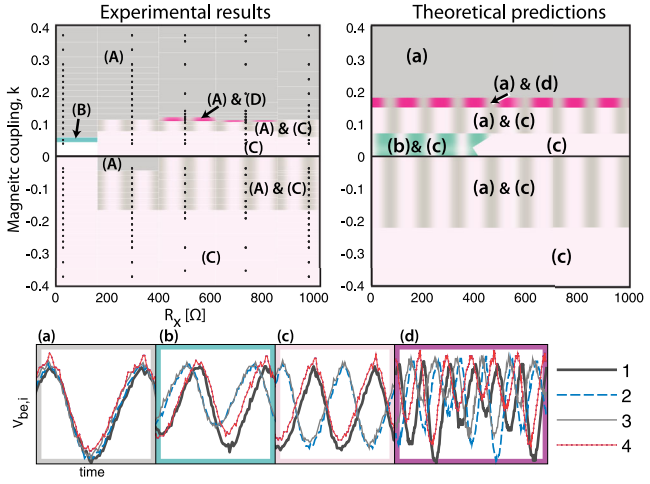

FIG. 4. Comparison between experimental results and theoretical predictions. Capital letters in figure indicate experimental observations; lowercase letters indicate theoretical predictions. [(A), (a), gray] one-cluster state; [(C), (c), pink] vertical two-cluster state; [(B), (b), turquoise] vertical two-cluster state two-cluster with a phase offset up to $\pi/2$; [(D), (d), magenta] quasi-periodic solution of the vertical two-cluster state; [white] no stable frequency locking. Stripes of two colors represent bistability between the two states represented by each color. (Top left) Experimentally observed cluster states. Black dots represent individual experimental measurements; we infer a color mesh from these results. (Top right) Theoretical prediction of cluster states from Fig. 3. (Bottom) Experimental time series of $V_{be}(t)$ demonstrating clusters corresponding to the theoretical predictions.

from the nine theoretical clustered patterns—[(a) gray] fully in phase, tolerating small mismatches in amplitude and phase, [(b), turquoise] the vertical two-cluster with a phase offset up to $\pi/2$ rad, [(c), pink] the vertical two-cluster, tolerating small mismatches in amplitude and phase, and [(d), magenta] the quasiperiodic vertical two-cluster, tolerating small mismatches in amplitude.

We performed experiments at five values of R_x (27Ω, 300Ω, 510Ω, 750Ω, and 1000Ω) and varied k from -0.03 to -0.4 for the parallel inductor configuration and from 0.03 to 0.4 for the antiparallel inductor configuration. To detect the presence of multiple attractors, we first increase then decrease k, guided by the theoretically predicted hysteresis between the periodic in-phase and the periodic antiphase solutions (in the left-hand panel of Fig. 3 no in-phase solution is present for large negative k, while in the right-hand panel no antiphase solution is present for large positive k). The top left-hand panel of Fig. 4 shows the cluster state observed at each experimental measurement.

Figure 4 shows broad agreement between our experimental and theoretical results (for discussion of the discrepancies, see the SM [32]). Each of the four cluster types (reported in the bottom boxes of Fig. 4) observed experimentally is predicted by the theoretical analysis. The system exhibits bistability between the fully synchronized state [(A), gray] and the vertical two-cluster state [(C), pink] for large ranges of k and R_x. We observe the fully synchronized solution for large positive magnetic coupling and small negative coupling; we observe the vertical two-cluster solution for small positive and large negative coupling. Near $k = 0.12$, we see the quasiperiodic vertical two-cluster state [(D), magenta]. At $k = 0.05$ and $R_x = 27\Omega$, we observe the vertical two-cluster with a phase separation near $\pi/2$ rad [(B), turquoise].

This work is the first study on cluster synchronization in multilayer networks with symmetries. We show that a small network with well-understood periodic Colpitts oscillators exhibits rich dynamical behavior such as bistability, hysteresis, and quasiperiodicity. This is the first experimental observation of a clustered quasiperiodic state. The analysis innovatively combines bifurcation analysis and the computation of transverse Lyapunov exponents, allowing us to overcome limitations of each individual approach. First, unlike the bifurcation analysis of the full system, our approach can handle multiple symmetries using standard software [44,46]. Second, compared to the computation of transverse Lyapunov exponents alone, it can find any possible cluster pattern even in the presence of multiple attractors of the quotient networks. The interplay of theory

and experiments was essential for an in-depth phenomenological understanding of the system behavior; experiments allowed us to understand which theoretically predicted cluster states were observable, while theory helped us identify hard to find cluster states. Note that even though we have applied our analysis to a very simple multilayer network, it is possible to scale the described approach to networks with any numbers of nodes or layers. This scaling is nontrivial and requires the definition of the group of symmetries of a multilayer network; this is the subject of ongoing research and is briefly introduced in the SM, Sec. V [32].

Our work shows how different interaction layers influence the overall state of the system; applications of the described theory can be found in a variety of fields where patterned behavior and multilayer systems arise. The method requires three ingredients: (1) a dynamical system describing the network, (2) multiple kinds of interactions, and (3) patterned behavior. Many papers propose dynamical equations for both neurons [50–52] and their network of interactions [53–56]; neurons are connected through electrical and chemical synapses [6]. A vast literature explores the likely relationship between epilepsy and synchronization [57], and models of coupled neurons exhibit clustered behavior [19]. Several models exist to describe the dynamics of opinion formation [58,59], which is mediated by different layers of interaction through social media, advertising, friend networks, etc., producing clusters of belief [60]. Bark beetles infest forests in patterns [61]; different tree species and various beetle transportation methods (self, carried by animals or wind, etc.) form the multilayer network representation of the forest-insect model [4]. Proposed circuit designs use quantum cellular automata with clusterlike clock zones to perform calculations; two kinds of quantum cellular automata cells (regular and rotated) are connected with either coplanar or multilayer connections [62]. Understanding the dynamical behavior of symmetric multilayer networks may play an important role in the design and development of neuromorphic computational systems [63]. To our knowledge, none of the studies on neuromorphic systems has considered dissimilar interactions between nodes, which seems to be an essential feature of most biological networks such as the brain [6] as well as a contributor to the overall robustness of a system [64,65].

This work was supported by the National Science Foundation (Grant No. 1727948).

*kb4hk@virginia.edu

[1] F. Ball and P. Neal, Network epidemic models with 308 two levels of mixing, Math. Biosci. **212**, 69 (2008).

[2] W. Wang, M. Tang, H. Yang, Y. Do, Y.-C. Lai, and G. Lee, Asymmetrically interacting spreading dynamics on complex layered networks, Sci. Rep. **4**, 5097 (2014).

[3] J. F. Padgett and C. K. Ansell, Robust Action and the Rise of the Medici, 1400-1434, Am. J. Sociology **98**, 1259 (1993).

[4] S. V. Buldyrev, R. Parshani, G. Paul, H. E. Stanley, and S. Havlin, Catastrophic cascade of failures in interdependent networks, Nature (London) **464**, 1025 (2010).

[5] V. Rosato, L. Issacharoff, F. Tiriticco, S. Meloni, S. D. Porcellinis, and R. Setola, Modelling interdependent infrastructures using interacting dynamical models, Int. J. Crit. Infrastruct. **4**, 63 (2008).

[6] A. E. Pereda, Electrical synapses and their functional interactions with chemical synapses, Nat. Rev. Neurosci. **15**, 250 (2014).

[7] B. M. Adhikari, A. Prasad, and M. Dhamala, Time delay-induced phase-transition to synchrony in coupled bursting neurons, Chaos **21**, 023116 (2011).

[8] X. Song, C. Wang, J. Ma, and J. Tang, Transition of electric activity of neurons induced by chemical and electric autapses, Sci. China: Technol. Sci. **58**, 1007 (2015).

[9] Y. Xiao, M. Xiong, W. Wang, and H. Wang, Emergence of symmetry in complex networks, Phys. Rev. E **77**, 066108 (2008).

[10] B. D. MacArthur, R. J. Sánchez-García, and J. W. Anderson, Symmetry in complex networks., Discrete Appl. Math. **156**, 3525 (2008).

[11] R. J. Sánchez-García, E. Cozzo, and Y. Moreno, Dimensionality reduction and spectral properties of multilayer networks, Phys. Rev. E **89**, 052815 (2014).

[12] M. De Domenico, V. Nicosia, A. Arenas, and V. Latora, Structural reducibility of multilayer networks, Nat. Commun. **6**, 6864 (2015).

[13] F. Sorrentino, Synchronization of a hypernetwork of coupled dynamical systems, New J. Phys. **14**, 033035 (2012).

[14] D. Irving and F. Sorrentino, Synchronization of a hypernetwork of coupled dynamical systems, Phys. Rev. E **86**, 056102 (2012).

[15] C. I. del Genio, J. Gómez-Gardeñes, I. Bonamassa, and S. Boccaletti, Synchronization in networks with multiple interaction layers, Sci. Adv. **2**, e1601679 (2016).

[16] R. Sevilla-Escoboza, I. Sendiña-Nadal, I. Leyva, R. Gutiérrez, J. M. Buldú, and S. Boccaletti, Interlayer synchronization in multiplex networks of identical layers, Chaos **26**, 065304 (2016).

[17] I. Leyva, R. Sevilla-Escoboza, I. Sendiña-Nadal, R. Gutiérrez, J. M. Buldú, and S. Boccaletti, Inter-layer synchronization in non- identical multi-layer networks, Sci. Rep. **7**, 45475 (2017).

[18] L. M. Pecora, F. Sorrentino, A. M. Hagerstrom, T. E. Murphy, and R. Roy, Cluster synchronization and isolated desynchronization in complex networks with symmetries, Nat. Commun. **5**, 4079 (2014).

[19] I. V. Belykh and M. Hasler, Mesoscale and clusters of synchrony in networks of bursting neurons, Chaos **21**, 016106 (2011).

[20] M. Wickramasinghe and I. Z. Kiss, Spatially Organized Dynamical States in Chemical Oscillator Networks: Synchronization, Dynamical Differentiation, and Chimera Patterns, PLoS One **8**, e80586 (2013).

[21] K. A. Blaha, J. Lehnert, A. Keane, T. Dahms, P. Hövel, E. Schöll, and J. L. Hudson, Clustering in delay-coupled

smooth and relaxational chemical oscillators, Phys. Rev. E **88**, 062915 (2013).
[22] N. E. Kouvaris, M. Sebek, A. S. Mikhailov, and I. Z. Kiss, Self-Organized Stationary Patterns in Networks of Bistable Chemical Reactions, Angew. Chem., Int. Ed. **55**, 13267 (2016).
[23] F. Sorrentino, L. M. Pecora, A. M. Hagerstrom, T. E. Murphy, and R. Roy, Complete characterization of stability of cluster synchronization in complex dynamical networks, Sci. Adv. **2**, e1501737 (2016).
[24] C. R. S. Williams, F. Sorrentino, T. E. Murphy, and R. Roy, Synchronization states and multistability in a ring of periodic oscillators: Experimentally variable coupling delays, Chaos **23**, 043117 (2013).
[25] L. Pecora, F. Sorrentino, A. Hagerstrom, T. Murphy, and R. Roy, Cluster synchronization and isolated desynchronization in complex networks with symmetries., Nat. Commun. **5**, 4079 (2014).
[26] M. Frasca, L. Gambuzza, A. Buscarino, and L. Fortuna, *Synchronization in Networks of Nonlinear Circuits* (Spinger International Publishing, Cham, Switzerland, 2018).
[27] M. Kennedy, Chaos in the Colpitts oscillator, IEEE Trans. Circuits Syst. **41**, 771 (1994).
[28] M. Kennedy, On the relationship between the chaotic Colpitts oscillator and Chua's oscillator, IEEE Trans. Circuits Syst. **42**, 376 (1995).
[29] G. M. Maggio, O. De Feo, and M. P. Kennedy, Nonlinear analysis of the Colpitts oscillator and applications to design, IEEE Trans. Circuits Syst. **46**, 1118 (1999).
[30] A. Uchida, M. Kawano, and S. Yoshimori, Dual synchronization of chaos in Colpitts electronic oscillators and its applications for communications, Phys. Rev. E **68**, 056207 (2003).
[31] L. K. Kana, A. Fomethe, H. B. Fotsin, E. T. Wembe, and A. I. Moukengue, Complex Dynamics and Synchronization in a System of Magnetically Coupled Colpitts Oscillators, J. Comp. Nonlin. Dyn. **2017**, 1 (2017).
[32] See Supplemental Material at http://link.aps.org/supplemental/10.1103/PhysRevLett.122.014101 for Sec. I—a full derivation and presentation of experimental parameters; Sec. II—an example on the smallest possible network; Sec. III—extra discussion of the analysis; Sec. IV—discussion of discrepancies between experiment and theory; and Sec. V—an in-depth discussion on the state of the field of multilayer network research, which includes Refs. [33–38].
[33] M. Berlingerio, M. Coscia, F. Giannotti, A. Monreale, and D. Pedreschi, Multidimensional networks: foundations of structural analysis, World Wide Web **16**, 567 (2013).
[34] S. V. Buldyrev, R. Parshani, G. Paul, H. E. Stanley, and S. Havlin, Catastrophic cascade of failures in interdependent networks, Nature (London) **464**, 1025 (2010).
[35] R. Criado, M. Romance, and M. Vela-Péerez, Hyperstructures, a new approach to complex systems, Int. J. Bifurcation Chaos Appl. Sci. Eng. **20**, 877 (2010).
[36] J. F. Donges, H. C. Schultz, N. Marwan, Y. Zou, and J. Kurths, Investigating the topology of interacting networks, Eur. Phys. J. B **84**, 635 (2011).
[37] J. Gao, S. V. Buldyrev, H. E. Stanley, and S. Havlin, Networks formed from interdependent networks, Nat. Phys. **8**, 40 (2012).
[38] S. Gomez, A. Diaz-Guilera, J. Gomez-Gardenes, C. J. Perez-Vicente, Y. Moreno, and A. Arenas, Diffusion dynamics on multiplex networks, Phys. Rev. Lett. **110**, 028701 (2013).
[39] M. Wickramasinghe and I. Z. Kiss, Synchronization of electrochemical oscillators with differential coupling, Phys. Rev. E **88**, 062911 (2013).
[40] M. Kivela, A. Arenas, M. Barthélémy, J. P. Gleeson, Y. Moreno, and M. A. Porter, Multilayer networks, J. Complex Netw. **2**, 203 (2014).
[41] S. Boccaletti, G. Bianconi, R. Criado, C. I. Del Genio, J. Gómez-Gardenes, M. Romance, I. Sendina-Nadal, Z. Wang, and M. Zanin, The structure and dynamics of multilayer networks, Phys. Rep. **544**, 1 (2014).
[42] M. Tinkham, *Group Theory and Quantum Mechanics* (McGraw-Hill, New York, 1964).
[43] Y. Xiao, B. D. MacArthur, H. Wang, M. Xiong, and W. Wang, Network quotients: Structural skeletons of complex systems, Phys. Rev. E **78**, 046102 (2008).
[44] E. J. Doedel, A. R. Champneys, F. Dercole, T. Fairgrieve, A. Yu, B. Oldeman, R. Paffenroth, B. Sandstede, X. Wang, C. Zhang *et al.*, Auto-07p: Continuation and bifurcation software for ordinary differential equations, http://www.hds.bme.hu/~fhegedus/BubbleDynamics/AUTO/auto.pdf.
[45] F. Dercole, Bpcont: An auto driver for the continuation of branch points of algebraic and boundary-value problems, SIAM J. Sci. Comput. **30**, 2405 (2008).
[46] A. Dhooge, W. Govaerts, and Y. A. Kuznetsov, Matcont: a matlab package for numerical bifurcation analysis of odes, ACM Trans. Math. Softw. **29**, 141 (2003).
[47] Y. A. Kuznetsov, W. Govaerts, E. J. Doedel, and A. Dhooge, Numerical periodic normalization for codim 1 bifurcations of limit cycles, SIAM J. Numer. Anal. **43**, 1407 (2005).
[48] V. D. Witte, F. D. Rossa, W. Govaerts, and Y. A. Kuznetsov, Numerical periodic normalization for codim 2 bifurcations of limit cycles: computational formulas, numerical implementation, and examples, SIAM J. Appl. Dyn. Syst. **12**, 722 (2013).
[49] E. Ott, *Chaos in Dynamical Systems* (Cambridge University Press, Cambridge, England, 2002).
[50] E. M. Izhikevich, *Dynamical Systems in Neuroscience* (MIT Press, Cambridge, MA, 2007).
[51] E. M. Izhikevich, Which Model to Use for Cortical Spiking Neurons?, IEEE Trans. Neural Networks **15**, 1063 (2004).
[52] C. Zhou and J. Kurths, Noise-induced synchronization and coherence resonance of a Hodgkin-Huxley model of thermally sensitive neurons, Chaos **13**, 401 (2003).
[53] J. W. Scannell, C. Blakemore, and M. P. Young, Analysis of connectivity in the cat cerebral cortex, J. Neurosci. **15**, 1463 (1995).
[54] O. Sporns and R. Kötter, Motifs in Brain Networks, PLoS Biol. **2**, 11 (2004).
[55] P. Hagmann, M. Kurant, X. Gigandet, P. Thiran, V. J. Wedeen, R. Meuli, and J.-P. Thiran, Mapping Human Whole-Brain Structural Networks with Diffusion MRI, PLoS One **2**, e597 (2007).

[56] E. T. Bullmore and D. S. Bassett, Brain Graphs: Graphical Models of the Human Brain Connectome, Annu. Rev. Clin. Psychol. **7**, 113 (2011).

[57] P. Jiruska, M. De Curtis, J. G. Jefferys, C. A. Schevon, S. J. Schiff, and K. Schindler, Synchronization and desynchronization in epilepsy: controversies and hypotheses, J. Physiol. **591**, 787 (2012).

[58] G. Deffuant, D. Neau, F. Amblard, and G. Weisbuch, Mixing beliefs among interacting agents, Adv. Complex Syst. **03**, 87 (2000).

[59] R. Hegselmann, U. Krause *et al.*, Opinion dynamics and bounded condence models, analysis, and simulation, J. Artif. Soc. Soc. Simul. **5** (2002).

[60] W. Quattrociocchi, G. Caldarelli, and A. Scala, Opinion dynamics on interacting networks: media competition and social inuence, Sci. Rep. **4**, 4938 (2014).

[61] F. Della Rossa, S. Fasani, and S. Rinaldi, Potential turing instability and application to plant-insect models, Math. Comput. Modell. **55**, 1562 (2012).

[62] H. Cho and E. E. Swartzlander, Adder designs and analyses for quantum-dot cellular automata, IEEE Trans. Nanotechnol. **6**, 374 (2007).

[63] J. Cosp, J. Madrenas, E. Alarcon, E. Vidal, and G. Villar, Synchronization of Nonlinear Electronic Oscillators for Neural Computation, IEEE Trans. Neural Networks **15**, 1315 (2004).

[64] M. Scheffer, S. R. Carpenter, T. M. Lenton, J. Bascompte, W. Brock, V. Dakos, J. van de Koppel, I. A. van de Leemput, S. A. Levin, E. H. van Nes, M. Pascual, and J. Vandermeer, Anticipating Critical Transitions, Science **338**, 344 (2012).

[65] M. Alberti, *Cities that Think like Planets: Complexity, Resilience, and Innovation in Hybrid Ecosystems* (University of Washington Press, Seattle, 2016).